JOURNAL OF Materials CHEMISTRY

Low temperature crystal structure of the organic metal ($[^2H_8]$BEDT–TTF)$_4Cl_2\cdot 6D_2O$ [BEDT–TTF = bis(ethylenedithio)tetrathiafulvalene]

Philippe Guionneau,*†[a] Cameron J. Kepert,[b] Matthew Rosseinsky,[b] Daniel Chasseau,[a] Jacques Gaultier,[a] Mohamedally Kurmoo,[c‡] Michael B. Hursthouse[d] and Peter Day[c]

[a]*Laboratoire de Cristallographie et Physique Cristalline, Université Bordeaux I, 351 cours de la Libération, F-33405 Talence Cedex, France*

[b]*Inorganic Chemistry Laboratory, South Parks Road, Oxford, UK OX1 3QR*

[c]*The Royal Institution of Great Britain, 21 Albemarle Street, London, UK W1X 4BS*

[d]*School of Chemistry and Applied Chemistry, University College of Wales, Cardiff, UK CF1 3TB*

($[^2H_8]$BEDT–TTF)$_4Cl_2\cdot 6D_2O$ [BEDT–TTF = bis(ethylenedithio)tetrathiafulvalene] exhibits a transition from semimetal to semiconductor at $T = 160$ K (Rosseinsky *et al*., *J. Mater. Chem*., 1993, **3**, 801). This electronic transition is accompanied by a structural transition that is characterized by the reversible appearance of superstructure reflections corresponding to the doubling of the cell parameter *b* and a change in space group from *Pcca* to *Pbcn*. The crystal structures are very similar above and below *T* and the calculated intermolecular transfer integrals scarcely change. In contrast, from the difference in intramolecular bond lengths, it is clear that the two crystallographically independent BEDT–TTF molecules carry different charges at low temperature, suggesting that a degree of ionicity arising in the BEDT–TTF layer is responsible for the change in electrical behaviour.

Progress in understanding the relation between the structures and properties of molecular materials has required the development of many new methods. For example, structure refinement by X-ray diffraction at low temperatures or high pressures is needed to shed light on the crystal structure at the points in the phase diagram where transformation takes place in physical properties. While high pressure X-ray investigations are still very rare,[1] low temperature crystal structure determination is increasingly accessible as a result of the introduction of area detectors, as evidenced by several recent publications.[2]

BEDT–TTF ($C_{10}H_8S_8$, also ET) salts have attracted great interest because of their diversity in physical properties due to extensive structural polymorphism. The chloride salts form an interesting set, $ET_3Cl_2\cdot 2H_2O$,[3] $ET_4Cl_2\cdot 4H_2O$[4] and $ET_3Cl_{2.5}\cdot H_5O_2$[5] are metallic under ambient conditions and undergo a transition towards a less conducting state at low temperature ($T_c = 100$, 50 and 70 K respectively), the 3:2 salt becoming superconducting at 5 K on applying a pressure of up to 0.5 GPa. The recently reported salt $ET_3Cl_2\cdot 5H_2O$[6] behaves as a semiconductor. ($[^2H_8]$ET)$_4Cl_2\cdot 6D_2O$ behaves as a semimetal[7] from room temperature ($\sigma = 40$ Scm^{-1}) to 160 K where a transition occurs towards a semiconducting state with a maximum activation energy of 30 meV. On applying pressure, the conductivity increases and the transition temperature decreases until the transition is suppressed at pressures greater than 2.4 GPa. The thermopower decreases linearly from room temperature to 160 K and then increases slightly. The magnetic susceptibility is low at room temperature and scarcely increases from 150 K to 50 K but then rises sharply down to 5 K. The room temperature crystal structure has been solved simultaneously by two groups showing that the deuterated salt, ($[^2H_8]$ET)$_4Cl_2\cdot 6D_2O$,[7] and the hydrogenated salt, $ET_4Cl_2\cdot 6H_2O$,[7] are isostructural but with structures very different from those of other ET chloride salts. They belong to the orthorhombic space group *Pcca*. The structural arrangement consists of columns of dimerized ET parallel to *c* that form layers parallel to the *bc* plane separated by anion sheets (Fig. 1). The main characteristic of the stacks is the alternation of parallel ET with twisted ET, the angle between dimers being about 30° (Fig. 2). The structure is therefore nearer to that of the α′-ET phase than that of the other ET salts with Cl anions. The intermolecular interactions are strong both within the chains and between adjacent stacks, indicating a strong 2D electronic behaviour. The Cl and O atoms of the anion layer create an unusual two-dimensional network formed by hydrogen bonds. In a previous paper,[9] we noted the need for structural information at low temperature to explain the mechanism of the electronic transition in this compound. Here, we present the temperature dependence of the crystal structure and the intermolecular electronic interactions of ($[^2H_8]$ET)$_4Cl_2\cdot 6D_2O$.

Experimental

The quality of each crystal was checked by X-ray diffraction on films before use. The crystals studied were black needles of approximate dimensions $1.4\times 0.4\times 0.2$ mm,[2] all of which had a small fraction of twinning.

The low temperature structural investigation of this salt was performed in two steps.

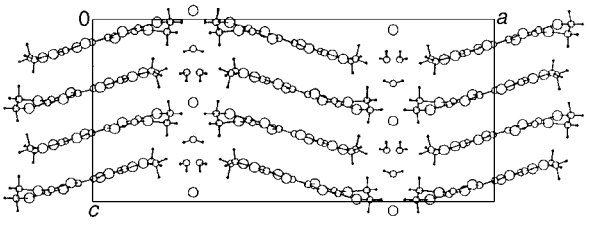

Fig. 1 View of the unit cell of ($[^2H_8]$ET)$_4Cl_2\cdot 6D_2O$ along *b*

*E-mail: Philippe.Guionneau@durham.ac.uk

† Durham Chemical Crystallography Group, Chemistry Department, Durham, UK DH1 3LE.

‡ Institut de Physique et Chimie des Materiaux de Strasbourg, CNRS-UMR 0046, 23 rue du Loess, 67037 Strasbourg Cedex, France.

At the University of Bordeaux I, evolution of the unit cell parameters was followed from 293 to 18 K with a three circle diffractometer equipped with a closed cycle helium cryostat. The angular positions of sets of eighteen Bragg reflections were determined at five fixed temperatures on cooling and refined to give the cell parameters. Fifteen sets were collected on warming. Data collection of the Bragg reflections was performed at 18 K, but the very low accuracy of the structural resolution factor ($R=16\%$), attributed to the quality of the crystals and to a technical problem leading to temperature fluctuations, does not permit us to present these results.

At the University College of Wales, Cardiff, we used a four circle diffractometer equipped with a nitrogen vapour jet cooling device operating down to 110 K and with a charge-coupled device (CCD) area detector. Strong superstructure reflections corresponding to the doubling of the *b* parameter were seen at low temperature during a fast preliminary investigation. Extended studies were performed on two crystals, in each case collecting complete structural data sets at 110 K and performing scans in ϕ at 5 K temperature increments to obtain the temperature-dependence of the superstructure intensities. Results for the two crystals were identical. The structure at 110 K was determined starting from the ambient temperature coordinates using SHELX76.[10] The D atoms of the ET extremities were fixed in theoretical positions and those of D_2O were refined from the room temperature positions. The moderately large magnitudes of the *R* and *Rw* factors (Table 1) and standard deviations of atomic coordinates may be attributed to the small fraction of twinning in the crystal.

Results and Discussion

Superstructure reflections

Analysis of the temperature-dependent intensities of more than 100 superlattice reflections shows that the transition displays no structural hysteresis. The temperature of appearance and disappearance of the reflections is about 165 K (Fig. 3), corresponding to the change in electrical behaviour ($T_c=160$ K). At 110 K, the temperature of the crystal structure determination, the superstructure reflection intensities are comparable to those of the main reflections. Hence, the crystal structure at 110 K correctly represents the structural evolution in the double cell.

The variation of I/I_{max} of representative reflections with (T/T_c) (Fig. 3) must be interpreted with caution because the values of I_{max} are estimated from the incomplete curve $I=f(T)$. The variation is quite steep when compared to the spin-Peierls system α'-ET_2X [X = $Ag(CN)_2$ and $AuBr_2$].[9,11]

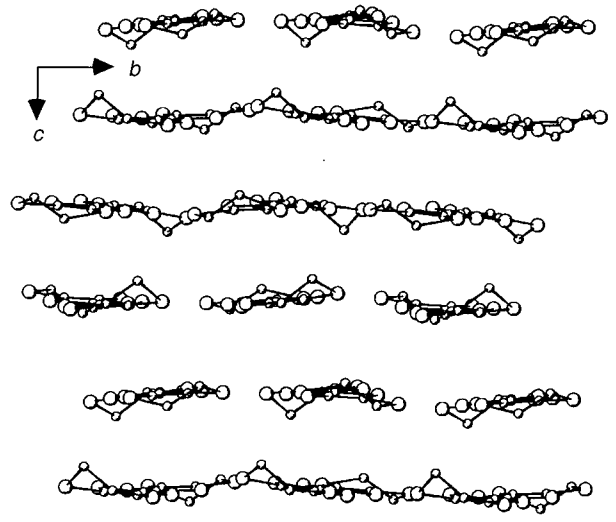

Fig. 2 View of the ET layer showing the ribbons of twisted dimers

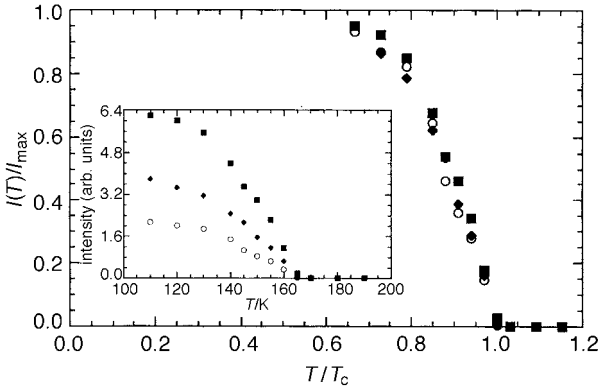

Fig. 3 Temperature dependence of the relative intensities of three superstructure reflections $I=f(T)$ and $I/I_{max}=f(T/T_c)$

We note that the conventional space group corresponding to the double cell is *Pbcn* but, in order to compare the structures at low and high temperatures, it is more convenient to use the non-standard space group *Pnca* that arises from *Pbcn* by rotating the axes.

Lattice parameter evolution

Fig. 4 shows the temperature dependence of the simple cell parameters of the title compound. There are no observable differences between the cell parameter values obtained on cooling or warming.

As shown previously for ET salts,[1,9,11] the main characteristic of the temperature dependence of the cell parameters is the anisotropy. Here, the relative variation of the parameter *c* (corresponding to the intrastack separation) is the highest, about twice as large as that for the interstack direction, *b*. The *a* parameter, which is perpendicular to the organic layers, remains nearly constant over the temperature range studied. The fact that the intrastack parameter decreases more than the interstack parameter mirrors the behaviour of α'-ET_2X[9] and $ET_3CuBr_2Y_2$ (Y = Cl or Br)[1] even if in those cases the most significant changes in conductivity occur in the interstack direction.

The temperature variation of the cell parameters changes markedly between 160 and 200 K with the onset of the superstructure reflections, so the choice of the temperature intervals is important in calculating the isobaric tensor. Thus the isobaric tensor was calculated over two temperature intervals (18–150 and 200–293 K) on either side of the transition zone. The principal components of the isobaric thermal expansion tensor are shown as a function of temperature in Fig. 5. The cell is orthorhombic and so the principal directions of expansion lie along the crystallographic axes. The amplitudes,

Table 1 Crystal and experimental data

$([^2H_8]ET)_4Cl_2\cdot 6D_2O$ temperature: 110 K			
Crystal system	orthorhombic	reflections:	
Space group	*Pnca*	for the cell	85
ET/cell	16	measured	19841
independent ET	2	independent	4838
a/Å	32.411(4)	observed	3158
b/Å	13.283(3)	parameters	349
c/Å	14.656(2)	$I/\sigma(I)$	3
V/Å^3	6309(4)	R_{int}	0.050
D/Mg m^{-3}	1.808	$R(F_o)$	0.064
$F(000)$	3464	$\omega R(F_o)$	0.061
Dimensions/mm	$1.4\times0.4\times0.2$		
λ/Å (Mo-Kα)	0.71069	observation:	twinned crystals
μ/mm^{-1}	1.162		

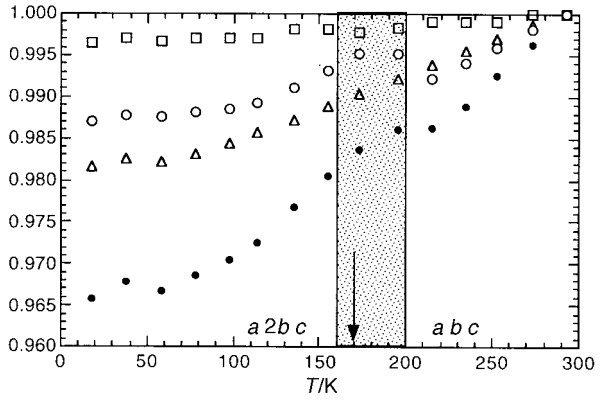

Fig. 4 Temperature dependence of the normalised lattice parameters: (□) a/a_0, (○) b/b_0, (△) c/c_0 and (●) V/V_0. Room temperature values are $a_0=32.497(15)$, $b_0=6.722(8)$, $c_0=14.826(8)$ Å and $V_0=3238(8)$ Å^3.

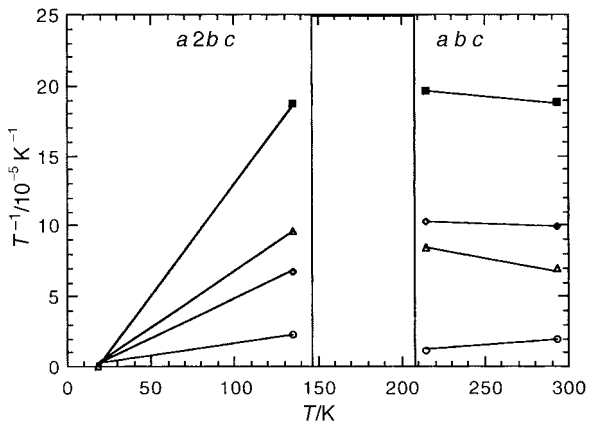

Fig. 5 Temperature dependence of components of the thermal expansion tensors

α_a, α_b and α_c vary very little from 293 to 200 K but change abruptly between 150 and 18 K. The three amplitudes become nearly zero at 18 K showing that the crystal is no longer thermally compressible.

At room temperature, the bulk modulus ($\alpha_V{}^{-1}$) is high, indicating a low compressibility. The value for the title compound (5300 K) is close to those of the α′-ET_2X salts (around 6000 K)[9] and much lower than that of ET_3CuBr_4 (9000 K).[1]

Crystal structure at low temperature

Below the structural transition temperature the unit cell is doubled without any change in the degree of symmetry. The transition therefore leads to the emergence of two crystallographically independent ET molecules, labelled A and B. At low temperature the ET stacks formed an …ABABA… sequence. In the simple cell there are five significant near neighbour interactions within each layer (Fig. 6) (*a*1, *a*2, *b*, *c*, *f*). It should be noted that the interactions of the type (x, y, z)−(1−x, −0.5+y, 0.5−z) are not considered significant owing to the very large intermolecular distances involved. The number of major interaction modes increases to eight in the doubled cell due to the existence of the two independent ET (*a*1, *a*2, *b*, *c*, *f*, *b*′, *c*′, *f*′). The stacks remain based on alternation of *a*1 and *a*2 in a manner that hardly changes from room temperature to 110 K: the averaged interplanar distances between the ET decrease from 3.69(1) to 3.63(1) Å (*a*1) and from 3.68(1) to 3.60(1) Å (*a*2) and the torsion angles from 0° to 1(1)° (*a*1) and 32(1)° to 30(1)° (*a*2). Table 3 lists the short interstack S−S distances (less than 1.2 times the sum of the van der Waal distances) and the angles formed by the S−S direction and the average ET plane. We recall that angles near zero lead to antibonding interactions.[11] The *b* interactions, corresponding to angles between the long axes of the ET molecules of around 30°, are quite weak and do not change at 110 K so the asymmetry introduced by *b* and *b*′ does not appear to be significant. The *c* interactions correspond to short distances that decrease at 110 K, the difference between *c* and *c*′ being significant but weak. The *f* interactions correspond to short distances and favourable angles for strong interactions. The transfer integrals corresponding to *f* and *f*′ are similar at low temperature. Hence, the intermolecular interactions appear a little stronger at low temperature, the salt retains its layer character and any irregularity caused by the structural differentiation between the two ET is minor.

The anionic layer consists of a two-dimensional network: Cl and O atoms linked by H-bonds form chains connected to each other by short O−Cl contacts. At low temperature, the distances within these chains scarcely decrease as the interchain O−Cl distances increase (Fig. 7). There are no close contacts between anions and cations either at room or low temperature,

Table 2 Averaged intramolecular bond lengths (Å) and charge for the two independent ET, A and B, at 110 K

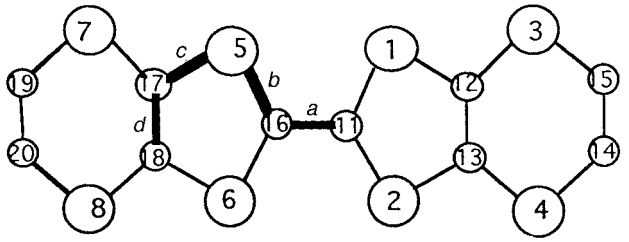

	a	*b*	*c*	*d*	*δ*	charge
293 K:	1.363	1.740	1.744	1.341	0.780	0.52
110 K:						
A	1.358	1.734	1.744	1.346	0.774	0.60
B	1.348	1.748	1.753	1.346	0.807	0.38

Table 3 Shortest intermolecular S−S distances (Å) with the contact angles [°] between ET of adjacent stacks. Standard deviations are less than 0.005 Å and 1.0°

Interactions	293 K	110 K
b	4.046 [54.9]	3.938 [53.2]
b′	as for *b*	3.969 [53.2]
		4.026 [51.1]
c	3.951 [5.8]	3.892 [7.9]
	3.466 [4.0]	3.492 [6.1]
	3.468 [4.6]	3.346 [6.4]
	3.892 [7.3]	3.839 [8.1]
	3.578 [11.1]	3.582 [12.1]
	3.476 [9.9]	3.434 [9.8]
c′	as for c	3.932 [8.1]
		3.384 [6.2]
		3.533 [6.0]
		3.880 [7.8]
		3.528 [11.9]
		3.503 [9.7]
f	4.054 [52.3]	4.034 [52.3]
	3.709 [57.1]	3.675 [58.1]
	3.858 [58.0]	3.909 [58.4]
	3.729 [64.5]	3.618 [65.3]
f′	as for *f*	4.024 [51.0]
		3.686 [57.1]
		3.773 [57.4]
		3.655 [63.2]

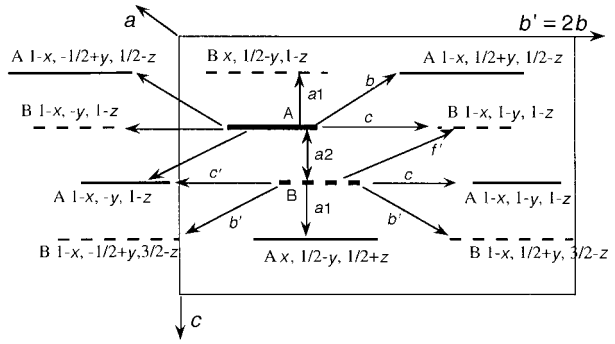

Fig. 6 Labelling scheme adopted for the ET layer in the double cell and the symmetry operations

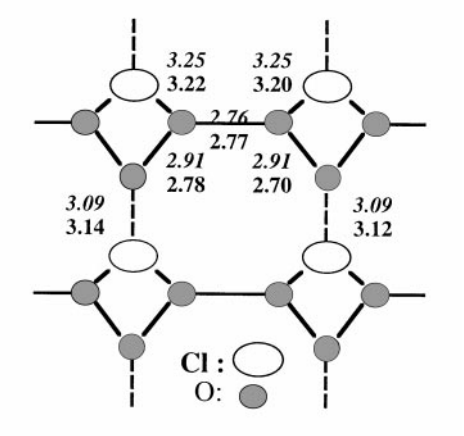

Fig. 7 Detail of the anion network and interatomic distances (Å) at 293 (italic) and 110 K

contrary to the situation found in the α′-ET_2X series or in ET_3CuBr_4.

Electronic interactions

The transfer integrals between neighbouring ET molecules have been calculated from the Hückel method using a double-ζ basis set[12] for both the room temperature and the low temperature structures (Table 4).

Results for the room temperature structure indicate that the intrachain interactions are quite strong but the degree of dimerization is high ($a1/a2 = 2.1$) and of the same order as that in the α′-ET_2X series. The interstack transfer integrals between coplanar ET are negative and comparable to the smaller intrachain one. The high value of the interstack transfer integral f confirms the two dimensional nature of this salt. It is interesting to note the coexistence between an intrachain dimerization tendency and a 2D character. At low temperature, the transfer integrals increase slightly. The intrastack dimerization does not increase below the transition, in contrast to $ET_3Cl_2{\cdot}2H_2O$ where the dimerization is more pronounced at low temperature. The emergence of two independent ET has little effect: the differences between f, f' and c, c' are quite small (20 meV) but agree with the change in electrical behaviour. The difference in the site energy of the two ET is an intermediate result in the dimer splitting calculations and arises from the difference in charge carried by the two ET. At room temperature this difference is zero because all the cations are identical, but at low temperature it increases to 60 meV as a result of the difference between A and B molecules. A similar variation has been found in the α′-ET_2X series and interpreted as the appearance of a degree of ionicity in the ET layers.

ET conformations and bond lengths

At room temperature, the two ethylene extremities of the ET are strongly disordered, as evidenced by the small bond lengths (1.381 and 1.389 Å instead of 1.53 Å) and large atomic thermal coefficients ($B_{eq} > 10$ Å^2) (Fig. 8). At 110 K, the ethylene groups of A and B are ordered indicating that the disorder observed at high temperature is dynamic: the values of these coefficients correspond to those expected at this temperature ($B_{eq} < 2.8$ Å^2)

Table 4 Values of the intermolecular transfer integrals (meV)

interactions		293 K	110 K
intrastack	$a1$	148	148
	$a2$	70	76
interstack	b	30	36
	b'	30	40
	c	−80	−100
	c'	−80	−80
	f	207	223
	f'	207	205

and the bond lengths are closer to the theoretical values. Such an ordering has been also observed in the α′-ET_2X series[9] and in $ET_3Cl_2{\cdot}3H_2O$.[13]

The central S−C and C=C bond lengths are quite different in A and B (Fig. 9). Recently we established a correlation between these intramolecular bond lengths and the charge of the ET.[14] This method, based on the parameter $\delta = (b+c)-(a+d)$ where b, c are the S−C and a, d the C=C averaged bond lengths of the central TTF (Table 2), enables the charge to be estimated with an accuracy of about 0.1 e. The structure refinement is good enough to use this method in the present case ($R < 8\%$ and standard deviations on bond lengths less than 0.01 Å). At room temperature the existence of a single crystallographically independent ET requires that

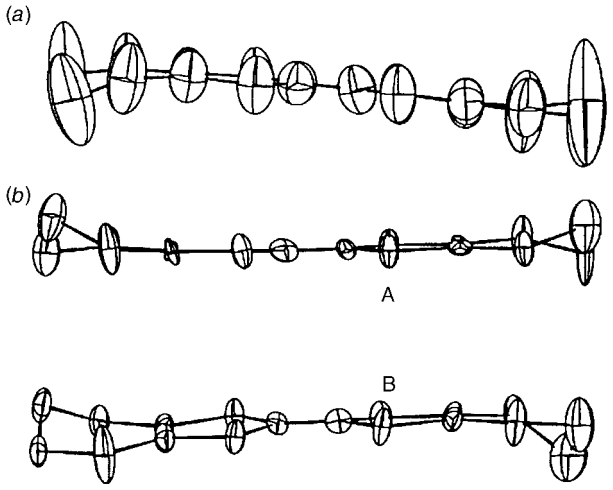

Fig. 8 Thermal ellipsoids (90% probability) of the ET molecules at (*a*) 293 and (*b*) 110 K

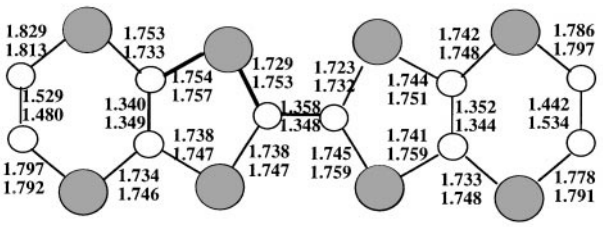

Fig. 9 Intramolecular bond lengths of the two independent ET (A and B) in $([^2H_8]ET)_4Cl_2{\cdot}6D_2O$ at 110 K. All standard deviations are less than 0.008 Å.

all the molecules carry a charge of $+1/2$, in agreement with the charge calculated by the δ-method [$+0.52(10)$]. We also note that the sum of the calculated charge for A and B at 110 K corresponds to that expected ($A+B=+0.98$ instead of $+1$). At 110 K, the S—C bonds in molecule A become shorter and the C=C longer than in B, corresponding to a difference in charge. From the δ-method we estimate that the charges in A and B at 110 K are respectively $+0.60(10)$ and $+0.38(10)$, a difference that is quite sufficient to open a gap at the Fermi energy and cause the transition from semimetal to semiconductor. An analogous phenomenon is observed in the α'-ET_2X series where a partial localization of the charges leads to similar values of the cation charges (in this case: 0.66 for one ET and 0.33 for the other at 120 K) below the transition towards a less conducting state.

Conclusions

The semimetal to semiconductor transition in ([$^2H_8$]-BEDT–TTF)$_4Cl_2\cdot 6D_2O$ is associated with a structural transition [(*Pcca, a, b, c*)<(*Pnca*, *a*, 2*b*, *c*)] that gives rise to an overall increase in the strength of the intermolecular interactions; the two dimensional character remains at low temperature. The change in physical properties is not caused by a molecular rearrangement but by the onset of a difference in ionicity between the two independent ET. Indeed, the main structural change resulting from the electronically driven transition is the distribution of bond lengths within the ET unit, which splits into two crystallographically independent units at low temperature. We believe that it is the separation in energy between the two independent ET, rather than any major changes in the intermolecular interactions, that is important in the development of a semiconducting band structure. The proposed mechanism for the semimetallic to semiconducting transition is a lowering of the free electron energy by band narrowing, which accompanies the separation of charge in the ET layer. Such a mechanism is analogous to the charge-density-wave induced metal to semiconductor transition. The analogy between the behaviour of the chloride and the α'-ET_2X series [$X=Ag(CN)_2$ or $AuBr_2$] is evident.

As the number of complete crystallographic studies at low temperature on this class of molecular conductors increases, it will be possible to correlate the transition in physical properties with the structural behaviour to extract general trends. From the results published up to now,[15] it is clear that cooling strongly influences the intramolecular conformation of the ET, the general outcome being the disappearance of the disorder in the ethylenic extremities and a change in the charge distribution.

We are grateful to Simon Coles for his help in Cardiff and to Laurent Ducasse for the transfer integrals calculation program. Financial support was received from the EPSRC (UK), the European Community (HCM network) and the Région Aquitaine (France).

References

1 P. Guionneau, J. Gaultier, D. Chasseau, G. Bravic, Y. Barrans, L. Ducasse, D. Kanazawa, P. Day and M. Kurmoo, *J. Phys. I Fr*., 1996, **6**, 1581.
2 See for example: T. Burgin, T. Miebach, J. C. Huffman, L. K. Montgomery, J. A. Paradis, C. Rovira, M.-H. Whangbo, S. N. Magonov. S. I. Khan, C. E. Strouse, D. L. Overmyer and J. E. Schirber, *J. Mater. Chem*., 1995, **5**(10), 1659; H. Kobayashi, K. Kawano, T. Naito and A. Kobayashi, *J. Mater. Chem*., 1995, **5**(10), 1681.
3 M. J. Rosseinsky, M. Kurmoo, D. R. Talham, P. Day and D. Watkin, *J. Chem. Soc. Chem. Commun*., 1988, 88.
4 R. P. Shibaeva, R. M. Lobkovskaya, L. P. Rozenberg, L. I. Burarov, A. A. Ignatiev, N. D. Kushch, E. E. Laukhina, M. K. Makova, E. B. Yagubskii and A. V. Zvarykina, *Synth. Met*., 1988, **27**, 189.
5 T. Mori and H. Inokuchi, *Bull. Chem. Soc. Jpn*., 1988, **61**, 591.
6 G. Ono, A. Izuoka, T. Sugawana and Y. Sugawana, *Mol. Cryst. Liq. Cryst*., 1996, **285**, 63.
7 M. J. Rosseinsky, M. Kurmoo, P. Day, I. R. Marsden, R.H. Friend, D. Chasseau, J. Gaultier, G. Bravic and L. Ducasse, *J. Mater. Chem*., 1993, **3**, 801.
8 M. B. Inoue, M. A. Bruck, M. Carducci and Q. Fernando, *Synth. Met*., 1990, **38**, 353.
9 P. Guionneau, J. Gaultier, M. Rahal, G. Bravic, J. M. Mellado, D. Chasseau, L. Ducasse, M. Kurmoo and P. Day, *J. Mater. Chem*., 1995, **5**, 1639
10 G. M. Sheldrick, SHELX 76, University of Cambridge, 1976.
11 D. Chasseau, J. Gaultier, G. Bravic, L. Ducasse, M. Kurmoo and P. Day, *Proc. R. Soc. Lond. A*, 1993, **442**, 207.
12 A. Fritsch and L. Ducasse, *J. Phys. I*, 1991, **1**, 855.
13 D. Chasseau, S. Hébrard, G. Bravic, J. Gaultier, L. Ducasse, M. Kurmoo and P. Day, *Synth. Met*., 1995, **70**, 947.
14 P. Guionneau, C. J. Kepert, D. Chasseau, M. R. Truter and P. Day, *Synth. Met*., 1997, **86**, 1973.
15 See *e.g.* ref. 2, 3, 9, 11, also V. E. Korotkov, V. N. Molchanov and R. P. Shibaeva, *Kristallografiya*, 1992, **37**, 1437. M. Fettouhi, L. Ouahab, D. Grandjean and L. Toupet, *Acta Crystallogr., Sect. B*., 1993, **49**, 685. M. Fettouhi, L. Ouahab, D. Grandjean and L. Toupet, *Acta Crystallogr. Sect. B*, 1992, **48**, 275. M. Kurmoo, A. W. Graham, P. Day, S. J. Coles, M. B. Hursthouse, J. M. Caulfield, J. Singleton, L. Ducasse and P. Guionneau, *J. Am. Chem. Soc*., 1995, **117**(49), 12 209.

Paper 7/04818A; *Received* 7*th July*, 1997